Rad18 and Rnf8 facilitate homologous recombination by two distinct mechanisms, promoting Rad51 focus formation and suppressing the toxic effect of nonhomologous end-joining

Shunsuke Kobayashi[1], Yohei Kasaishi[1], Shinichiro Nakada[2, 3], Tokiyo Takagi[4], Saho Era[1], Akira Motegi[1], Roland K. Chiu[5], Shunichi Takeda[1], and Kouji Hirota[1, 4]

[1]Department of Radiation Genetics, Kyoto University Graduate School of Medicine, Yoshida Konoe, Sakyo-ku, Kyoto 606-8501, Japan
[2]Center of Integrated Medical Research, School of Medicine, Keio University, Tokyo 160-8582, Japan
[3]Present address: Department of Bioregulation and Cellular Response, Graduate School of Medicine, Osaka University, Osaka, Japan
[4] Department of Chemistry, Graduate School of Science and Engineering, Tokyo Metropolitan University, Minamiosawa 1-1, Hachioji-shi, 192-0397, Tokyo
[5] Department of Cell Biology, Department of Radiation Oncology, University of Groningen, University Medical Center Groningen, Groningen, The Netherland

Address correspondence to Kouji Hirota and Shunichi Takeda
Department of Radiation Genetics, Kyoto University, Graduate School of Medicine, Yoshida Konoe, Sakyo-ku, Kyoto 606-8501, Japan
Tel: 81-75-753-4411, Fax: 81-75-753-4419
Correspondence to Kouji Hirota, khirota@rg.med.kyoto-u.ac.jp, or Shunichi Takeda, stakeda@rg.med.kyoto-u.ac.jp.
(Shunichi Takeda is designated for editorial queries.)
Functional relationship between RAD18 and RNF8 in HR

None of the authors have any conflicts of interest associated with this study.
3740 words

Abstract

The E2 ubiquitin conjugating enzyme Ubc13 and the E3 ubiquitin ligases Rad18 and Rnf8 promote homologous recombination (HR) mediated double-strand break (DSB) repair by enhancing polymerization of the Rad51 recombinase at γ-ray-induced DSB sites. To analyze functional interactions between the three enzymes, we created *RAD18*$^{-/-}$, *RNF8*$^{-/-}$, *RAD18*$^{-/-}$/*RNF8*$^{-/-}$ and *UBC13*$^{-/-}$ clones in chicken DT40 cells. To assess the capability of HR, we measured the cellular sensitivity to camptothecin (topoisomerase I poison) and olaparib (poly[ADP ribose]polymerase inhibitor) because these chemotherapeutic agents induce DSBs during DNA replication, which are repaired exclusively by HR. *RAD18*$^{-/-}$, *RNF8*$^{-/-}$ and *RAD18*$^{-/-}$/*RNF8*$^{-/-}$ clones showed very similar levels of hypersensitivity, indicating that Rad18 and Rnf8 operate in the same pathway in the promotion of HR. Although these three mutants show less prominent defects in the formation of Rad51 foci than *UBC13*$^{-/-}$ cells, they are more sensitive to camptothecin and olaparib than *UBC13*$^{-/-}$ cells. Thus, Rad18 and Rnf8 promote HR-dependent repair in a manner distinct from Ubc13. Remarkably, deletion of Ku70, a protein essential for nonhomologous end-joining (NHEJ) significantly restored tolerance of *RAD18*$^{-/-}$ and *RNF8*$^{-/-}$ cells to camptothecin and olaparib without affecting Rad51 focus formation. Thus, in cellular tolerance to the chemotherapeutic agents, the two enzymes collaboratively promote DSB repair by HR by suppressing the toxic effect of NHEJ on HR rather than enhancing Rad51 focus formation. By contrast, following exposure to γ-rays *RAD18*$^{-/-}$, *RNF8*$^{-/-}$, *RAD18*$^{-/-}$/*RNF8*$^{-/-}$ and *UBC13*$^{-/-}$ cells showed close correlation between cellular survival and Rad51 focus formation at DSB sites. In summary, the current study reveals that Rad18 and Rnf8 facilitate HR by two distinct mechanisms: suppression of the toxic effect of NHEJ on HR during DNA replication; and the promotion of Rad51 focus formation at radiotherapy-induced DSB sites. (286 words)

Running title (not more than 50 letters and space)

Functional relationship between RAD18 and RNF8 in HR

Six descriptive key words

E3 ubiquitin ligases, Rad18, Rnf8, Double strand break (DSB), Homologous recombination (HR), Nonhomologous end-joining (NHEJ).

Introduction

Anti-cancer therapeutic DNA damaging agents including ionizing radiation, camptothecin (a topoisomerase I poison) and olaparib (an inhibitor against poly[ADP ribose]polymerase) kill cycling cells by inducing DSBs. These agents create DSBs in distinct manners, as ionizing radiation generates DSBs in genomic DNA in a higher order chromatin structure, while camptothecin and olaparib generate DSBs in one of two sister chromatids during DNA replication. Ionizing-radiation-induced DSBs are repaired by both homologous recombination (HR) and nonhomologous end-joining (NHEJ) [1-4], while DSBs induced by camptothecin and olaparib are repaired exclusively by HR [5-9]. The two DSB repair pathways compete with each other as evidenced by the observation that the embryonic mortality caused by a defect in the HR factor BRCA1 is suppressed by the additional mutation of 53BP1, a factor involved in NHEJ [10].

Vital roles for Rad18 and Rnf8 in genome maintenance have been suggested from a number of studies on cells treated with siRNA for transient depletion of Rad18 or Rnf8. However, the strong effects caused by such transient depletion require careful interpretation as both the *RAD18*$^{-/-}$ and *RNF8*$^{-/-}$ mice develop normally without showing prominent defects in meiotic HR or NHEJ-dependent V(D)J recombination in lymphoid precursors [11-15]. Lack of any prominent phenotype in these mice is partly attributable to difficulty in precise phenotypic analysis of DNA damage response using primary culture cells. Moreover, the acute effect caused by siRNA-mediated transient depletion can be greater than the long-term effect caused by loss of functional proteins, due to compensation for the loss by up-regulation of other proteins in the long term. To analyze the effects caused by the loss of ubiquitylation enzymes involved in DNA damage responses, we have generated isogenic mutants from a single parental cell line, DT40 cells. In addition, to precisely distinguish the catalytic role from the non-ubiquitylation role of Rad18 and Rnf8, we created ubiquitylation-dead mutants (*RAD18*$^{C29F/-}$ and *RNF8*$^{C398F/-}$ cells) as well as *null* mutants (*RAD18*$^{-/-}$ and *RNF8*$^{-/-}$ cells) (Table 1).

In this study, we analyzed the capability of *RAD18*$^{-/-}$, *RNF8*$^{-/-}$, *RAD18*$^{-/-}$ */RNF8*$^{-/-}$ and *UBC13*$^{-/-}$ clones to perform HR to repair DSBs, and made the following three conclusions. First, Rad18 and Rnf8 facilitate DSB repair by HR using two distinct mechanisms: promoting Rad51 focus formation at γ-ray-induced DSB sites; and suppressing the toxic effect of NHEJ on HR during the repair of DSBs induced by

camptothecin and olaparib. Second, Rad18 and Rnf8 promote Rad51 focus formation independently of each other, while the two enzymes function in the same pathway in suppressing the toxic effect of NHEJ on HR. Third, the non-catalytic functioning of Rad18 and Rnf8 significantly contributes to Rad51 focus formation.

Results

RNF8$^{-/-}$ and *UBC13*$^{-/-}$ cells display distinctly different phenotypes

To disrupt the chicken *RNF8* locus, we constructed two targeting vectors, *RNF8-puro* and *RNF8-bsr* (Supplementary Figure 1A), and sequentially transfected these constructs into *wild-type* DT40 cells. Targeted disruption of the *RNF8* gene was verified by Southern blot analysis of *Xba*I-digested genomic DNA with the use of an external 3' probe (Supplementary Figure 1B). RT-PCR analysis showed loss of RNF8 expression confirming disruption of the *RNF8* gene (Supplementary Figure 1C). *RNF8*$^{-/-}$ cells proliferated with normal kinetics, while *UBC13*$^{-/-}$ cells proliferated with slower kinetics due to spontaneously occurring apoptosis, compared with *wild-type* cells [16] (Figure 1A). The extent of apoptosis during the cell cycle was closely correlated with the number of spontaneously arising mitotic chromosomal breaks among isogenic DNA-repair-deficient DT40 mutants [17]. In agreement with the close correlation, *RNF8*$^{-/-}$ cells exhibited no increase in the number of spontaneous chromosomal breaks, while *UBC13*$^{-/-}$ cells exhibit a significant increase (Figure 1B). The severe genome instability of *UBC13*$^{-/-}$ cells agrees with the embryonic lethality of *UBC13*$^{-/-}$ mice [18, 19]. These observations indicate that Ubc13 is able to contribute to genome maintenance independently of Rnf8.

To determine in which DNA repair pathways Rnf8 plays a role, we measured cellular survival after exposure of cells to DNA-damaging agents. *KU70*$^{-/-}$ cells but not *RNF8*$^{-/-}$ cells were sensitive to ICRF193 [20, 21], a catalytic inhibitor of topoisomerase II (Figure 1C), indicating that Rnf8 is not involved in the promotion of canonical NHEJ. We then measured sensitivity to camptothecin (a topoisomerase I poison) and olaparib (a poly [ADP- ribose] polymerase inhibitor), two chemotherapeutic agents that induce replication fork collapse. The subsequent restart of replication requires HR with the intact sister chromatid [5-9]. *RNF8*$^{-/-}$ cells showed greater sensitivity to both camptothecin and olaparib than *UBC13*$^{-/-}$ cells, and the sensitivity was completely reversed by complementation with a *RNF8* transgene (Supplementary Figure 1D-F). The

hypersensitivity in *RNF8*$^{-/-}$ cells to camptothecin is consistent with results of a previous study [22]. From the data of Figure 1D and E, we conclude that Rnf8 can function independently of Ubc13 in the cellular tolerance to the chemotherapeutic agents.

The Rad18 and Rnf8 ubiquitin ligases are compensatory for each other in genome maintenance and promotion of Rad51 polymerization at γ-ray-induced DSB sites

To analyze the functional relationship between Rad18 and Rnf8, we generated *RAD18*$^{-/-}$*/RNF8*$^{-/-}$ double mutant cells. Spontaneously arising chromosome breaks in *RAD18*$^{-/-}$*/RNF8*$^{-/-}$ double mutant were increased 4-fold as compared with either *RAD18*$^{-/-}$ or *RNF8*$^{-/-}$ single mutant cells (Figure 1B). This result reveals substantial functional redundancy between Rad18 and Rnf8 in genome maintenance during the cell cycle.

We next measured sensitivity of *RAD18*$^{-/-}$*/RNF8*$^{-/-}$ cells to ICRF193, camptothecin, olaparib, and γ-rays. *RAD18*$^{-/-}$, *RNF8*$^{-/-}$ and *RAD18*$^{-/-}$*/RNF8*$^{-/-}$ cells showed no sensitivity to ICRF193 (Figure 2A), however they were similarly sensitive to camptothecin (Figure 2B). Moreover, the three types of cells showed similar sensitivity to olaparib (Figure 2C). In sharp contrast, *RAD18*$^{-/-}$*/RNF8*$^{-/-}$ cells showed significantly greater sensitivity to γ-rays than observed with *RAD18*$^{-/-}$ or *RNF8*$^{-/-}$ cells (Figure 2D). We therefore conclude that Rad18 and Rnf8 ubiquitin ligases operate in the same pathway in HR-mediated repair of DSBs induced by the two chemotherapeutic agents, while Rad18 and Rnf8 can facilitate HR-mediated repair of γ-ray-induced DSBs independently of one another. To explore the role of the two ubiquitin ligases in HR, we measured Rad51 focus formation following γ-rays irradiation. The Rad51 focus formation of *RAD18*$^{-/-}$*/RNF8*$^{-/-}$ cells was reduced 2.5 fold as compared with either *RAD18*$^{-/-}$ or *RNF8*$^{-/-}$ cells (Figure 2E and Supplementary Figure 2B). This phenotype agrees with the γ-ray sensitivity of *RAD18*$^{-/-}$, *RNF8*$^{-/-}$ and *RAD18*$^{-/-}$*/RNF8*$^{-/-}$ cells. Thus, the two ubiquitin ligases independently promote the function of Rad51 at γ-ray-induced DSBs.

To investigate whether the functional redundancy seen in the DT40 clones were relevant to human cells, we analyzed γ-ray-induced Rad51 focus formation in human HCT116 cells. The depletion of Rnf8 was assessed by analyzing the disappearance of 53BP1 foci [23-25] (Supplementary Figure 3). Similar to the observation in *RAD18*$^{-/-}$ mouse embryonic fibroblasts [26], *RAD18*$^{-/-}$ HCT116 cells displayed only a slight defect in Rad51 focus formation. Although the depletion of Rnf8 caused only a mild reduction

of Rad51 foci formation in the *RAD18*$^{+/+}$ HCT116 cells, it significantly decreased the number of Rad51 foci in the *RAD18*$^{-/-}$ cells (Figure 2F and Supplementary Figure 3). We therefore conclude that Rad18 and Rnf8 independently contribute to the Rad51 focus formation at γ-ray-induced DSBs in the chicken and human cells.

The inactivation of NHEJ in *RNF8*$^{-/-}$ and *RAD18*$^{-/-}$ cells significantly restores their tolerance to camptothecin and olaparib

The epistatic relationship between *RAD18* and *RNF8* in cellular tolerance to camptothecin and olaparib (Figure 2B and C) led us to investigate whether Rnf8 suppresses the toxic effect of NHEJ on HR as does Rad18 [3]. We inactivated NHEJ by disrupting the *KU70* gene in *RNF8*$^{-/-}$ cells, and found that loss of Ku70 in *RNF8*$^{-/-}$ as well as *RAD18*$^{-/-}$ cells completely restored their cellular tolerance to camptothecin (Figure 3A). Similarly, *RNF8*$^{-/-}$*/KU70*$^{-/-}$ and *RAD18*$^{-/-}$*/KU70*$^{-/-}$ cells were more tolerant to olaparib than *RAD18*$^{-/-}$ and *RNF8*$^{-/-}$ cells (Figure 3B). Thus, Rad18 and Rnf8 might suppress the toxic effect of NHEJ on HR. To verify that the observed cellular tolerance represents the capability of cells to repair one-end breaks, which occur as a consequence of replication over broken template strands, we examined chromosomal aberrations in mitotic cells having been treated with camptothecin. *RNF8*$^{-/-}$ and *RAD18*$^{-/-}$ cells showed significant increases in the number of chromosomal aberrations compared to *wild-type* cells, while such increases were not seen in *RNF8*$^{-/-}$*/KU70*$^{-/-}$ and *RAD18*$^{-/-}$*/KU70*$^{-/-}$ cells (Figure 3C). Thus, cellular survival (Figure 3A) represents the capability of cells to repair one-end breaks. Taken together, we conclude that collaboration between Rad18 and Rnf8 suppresses the toxic effect of NHEJ on HR-dependent repair of one-end breaks (Figure 3C).

There are three possible mechanisms underlying the toxic effect by NHEJ. The Ku proteins might suppress HR by inhibiting the polymerization of Rad51 at one-end breaks or by interfering with subsequent steps such as homology search and strand exchange. The third mechanism involves aberrant NHEJ of two one-end breaks derived from neighboring stalled replication forks. We measured Rad51 focus formation following exposure of cells to camptothecin, and found that the loss of Ku70 did not restore the Rad51 focus formation of *RNF8*$^{-/-}$ cells (Figure 3D and Supplementary Figure 2A). Thus, Rnf8 suppresses the toxic effect of NHEJ on HR presumably by facilitating homology search and/or strand exchange. To address the third mechanism,

we counted the number of radial chromosomes (Figure 3C, E and F), which arises mainly as a consequence of aberrant NHEJ [10], as NHEJ-deficient *KU70*$^{-/-}$ cells exhibited a few times lower radial chromosomes events than *wild-type* cells (Figure 3F). The number of radial chromosomes in *RAD18*$^{-/-}$/*RNF8*$^{-/-}$ cells was very similar to that in *RNF8*$^{-/-}$ and *RAD18*$^{-/-}$ cells. Strikingly, the loss of Ku70 in *RNF8*$^{-/-}$ and *RAD18*$^{-/-}$ cells greatly reduced the number of radial chromosomes (Figure 3C and F). We conclude that Rad18 and Rnf8 work together to promote HR-dependent repair of one-end breaks by inhibiting both aberrant NHEJ of two one-end breaks and a suppressive effect of NHEJ on HR.

In summary, Rnf8 and Rad18 facilitate HR in two distinctly different ways, the promotion of Rad51 polymerization at DSB sites and suppression of the toxic effect by NHEJ on HR. Moreover, the functional relationship between Rad18 and Rnf8 differs depending on DNA-damaging agents, as the two enzymes are compensatory for each other in the promotion of Rad51 polymerization at γ-ray-induced DSBs while the two enzymes operate in the same pathway in maintaining replication fork progression when cells are exposed to camptothecin and olaparib.

The ubiquitylation activity of Rad18 and Rnf8 is essential for cellular tolerance to camptothecin and olaparib

Accumulating evidence has suggested a non-catalytic (non-ubiquitylation) function of Rad18 and Rnf8 in the initial step of HR dependent DSB repair [26-28]. To address possible non-ubiquitylation roles of Rad18 and Rnf8, we selectively inactivated the ubiquitylation activity by mutating C398F and C29F in the *RNF8* and *RAD18* genes, respectively [26, 27, 29], and generated *RNF8*$^{C398F/-}$ (Supplementary Figure 4A), *RAD18*$^{C29F/-}$ (Supplementary Figure 5A), *RAD18*$^{-/-}$/*RNF8*$^{C398F/-}$ and *RNF8*$^{-/-}$/*RAD18*$^{C29F/-}$ clones. The *RNF8* and *RAD18* knock-in mutations were confirmed by RT-PCR (Supplementary Figure 4B and 5B) and sequence analysis. The C398F mutation completely inactivates the ubiquitylation activity of Rnf8, since *RNF8*$^{C398F/-}$ as well as *RNF8*$^{-/-}$ cells showed no ubiquitin foci at γ-ray-induced DSB sites (Supplementary Figure 4C). The C29F mutation also inhibits the ubiquitylation activity of Rad18, since UV-induced mono-ubiquitylation of PCNA was not increased in *RAD18*$^{C29F/-}$ or *RAD18*$^{-/-}$ cells (Supplementary Figure 5C).

We first evaluated the effects of the C29F and C398F mutations on the

maintenance of genome integrity (Figure 1B). The number of spontaneously arising mitotic chromosomal breaks in *RNF8*$^{-/-}$/*RAD18*$^{C29F/-}$ and *RAD18*$^{-/-}$/*RNF8*$^{C398F/-}$ clones was very similar to that in *RAD18*$^{-/-}$/*RNF8*$^{-/-}$ cells, indicating that the catalytic functioning of the two enzymes is critical for genome stability. Next we evaluated the effects of the C29F and C398F mutations on the cellular tolerance to camptothecin and olaparib (Figure 4A and B). The C29F and C398F mutations had the same effect on the cellular tolerance to both camptothecin and olaparib, as did the null mutations of the *RAD18* and *RNF8* genes (Figure 4A and B). Therefore, the ubiquitylation activity of both Rad18 and Rnf8 is essential for repressing the toxic effect of NHEJ on HR-dependent DSB repair.

The contribution of non-ubiquitylation roles played by Rad18 and Rnf8 in initiating HR at γ-ray-induced DSB sites

We next evaluated non-catalytic functions of Rad18 and Rnf8 in the repair of γ-ray-induced DSBs as well as γ-ray-induced Rad51 focus formation. The *RAD18* C29F mutation had the same effect on γ-ray-sensitivity as the *RAD18*$^{-/-}$ *null* mutation (Figure 4C). Similarly, the *RNF8* C398F mutation had the same effect on γ-ray-sensitivity as the *RNF8*$^{-/-}$ *null* mutation (Figure 4C). Thus, non-ubiquitylation roles played by Rad18 and Rnf8 contribute only marginally, if any, to HR-dependent repair of γ-ray-induced DSBs. To assess the role of ubiquitylation by Rnf8 in Rad51 focus formation, we counted the number of Rad51 foci in ionizing irradiation treated *RAD18*$^{-/-}$, *RAD18*$^{-/-}$/*RNF8*$^{C398F/-}$ and *RAD18*$^{-/-}$/*RNF8*$^{-/-}$ clones after one hour. The Rad51 focus formation of *RAD18*$^{-/-}$/*RNF8*$^{C398F/-}$ cells was lower than that of *RAD18*$^{-/-}$ cells while higher than *RAD18*$^{-/-}$/*RNF8*$^{-/-}$ cells (Figure 4D). This result indicates that Rnf8 promotes Rad51 polymerization through both non-catalytic and protein ubiquitylation, as suggested previously [27], particularly when Rad18 is absent. Similarly, the Rad51 focus formation of *RNF8*$^{-/-}$/*RAD18*$^{C29F/-}$ cells was an intermediate between those of *RNF8*$^{-/-}$ and *RAD18*$^{-/-}$/*RNF8*$^{-/-}$ clones (Figure 4D and Supplementary Figure 2B), indicating that the non-catalytic function of Rad18 plays an important role in Rad51 focus formation.

Discussion

In this study, we demonstrated that Rad18 and Rnf8 facilitate HR by two distinct mechanisms, promotion of Rad51 focus formation and suppression of the toxic effect of

NHEJ on HR. The latter mechanism does not require the promotion of Rad51 focus formation as the loss of Ku70 reversed the cellular tolerance of *RNF8*$^{-/-}$ cells to camptothecin without changing Rad51 focus formation (Figure 3D). Thus, Rad18 and Rnf8 contribute to cellular tolerance to anti-malignant therapies with more complex mechanism than previously appreciated.

We also revealed complex functional relationships between the Rad18 and Rnf8 ubiquitin ligases. The two enzymes operate in the same pathway in cellular tolerance to camptothecin and olaparib (Figure 2B and C), while they work independently in both cellular tolerance to radiotherapy (Figure 2D) and promoting the function of Rad51 at DSBs induced by γ-rays (Figure 2E and F). Moreover, the catalytic role of Rad18 and Rnf8 is required for the cellular tolerance to camptothecin, olaparib and radiotherapy (Figure 4A to C), while the non-catalytic function of both enzymes contributed to Rad51 focus formation (Figure 4D). In summary, the functional relationship between Rad18 and Rnf8 in DNA damage responses is distinctly different depending on the type of DNA damage.

Although a large number of studies previously suggested pivotal roles of Rad18 and Rnf8 in DNA damage responses, mice deficient in either Rad18 or Rnf8 display only modest phenotypes and are capable of performing meiotic HR [13, 30]. The moderate phenotypes imply that other related enzymes potentially compensate for the absence of Rad18 or Rnf8. We demonstrated in this study that the two enzymes compensate for one another in the maintenance of chromosomal DNA, as only *RAD18*$^{-/-}$*/RNF8*$^{-/-}$ cells but not *RAD18*$^{-/-}$ or *RNF8*$^{-/-}$ cells showed severe genome instability (Figure 1B) as observed in *UBC13*$^{-/-}$ cells [16]. Conceivably, the dramatic phenotype of *RAD18*$^{-/-}$*/RNF8*$^{-/-}$ and *UBC13*$^{-/-}$ cells results from combined defects of HR-dependent DSB repair coupled with defects in post-replicational repair. In summary, Rad18 and Rnf8 have a substantially redundant role in genome maintenance.

HR plays a dominant role over NHEJ in DSB repair of *Saccharomyces cerevisiae*, whereas HR and NHEJ contribute equally to the whole DSB repair outcome in metazoan cells. Given that in metazoans, a DSB is targeted by both HR and NHEJ, the two pathways could potentially interfere with each other and prevent effective DSB repair (reviewed in Chapman *et al* [31]). To avoid such interference, NHEJ must be actively inhibited, in particular for the repair of the DSBs that occur in one of two sister chromatids during DNA replication. This is because camptothecin and olaparib induce

numerous DSBs associated with replication, which DSBs are repaired accurately by HR but not by NHEJ. Recent study has reported that the loss of 53BP1 in Brca1-deficient cells rescues HR defect, indicating that Brca1 antagonizes 53BP1 and promotes end resection in S phase [10]. Our current study further revealed that a collaboration between Rad18 and Rnf8 prevent the function of NHEJ and thereby facilitates HR-mediated repair of DSBs induced by camptothecin and olaparib. Moreover, NHEJ causes an increase in the number of radial chromosomes in both *RNF8*$^{-/-}$ and *RAD18*$^{-/-}$ cells (Figure 3C and F). We also revealed that the inhibition of NHEJ requires functional ubiquitylation capability of the two enzymes (Figure 4A and B), perhaps mono-ubiquitylation by Rad18 followed by poly-ubiquitylation by Rnf8. The precise identity of the Rad18 and Rnf8 ubiquitylation substrate remains an important unresolved question. Although ubiquitylation of 53BP1, Ku80 and proteins involved in the Fanconi anemia pathway by Rad18 [32, 33] was reported, they might not contribute to cellular tolerance to camptothecin and olaparib. The rationale for this is because 53BP1 and Ku80 could repress an initial step of HR whereas Rad18 and Rnf8 inhibit the toxic effect of NHEJ on HR without affecting Rad51 focus formation (Figure 3D). Future studies are required to identify substrates for ubiquitylation as well as the structure of ubiquitylation at various DNA lesions.

Materials and methods

Plasmid construction

For disrupting the *RNF8* gene, *RNF8-puro*, *RNF8-bsr*, and *RNF8-neo* were generated from genomic PCR products using the primers 5'-GTAACTGTAGGCCGGGGATTAGATCTCACG-3' and 5'-CGGCTCAGTTCTTCCATCAGAGCATGATGC-3'. Amplified PCR products were cloned into the pCRII-TOPO vector (Invitrogen, CA). The 5.3kb *Xba*I fragment from the cloned PCR amplified region was further subcloned into the *Xba*I site of the pBluescriptII KS (+) vector. Each marker-gene cassette was ligated into the *Bam*HI site that corresponds to the 86th amino-acid residue of the *RNF8* coding sequence. The 1.2kb fragment from genomic DNA amplified using the primers 5'-GCATCATGCTCTGATGGAAGAACTGAGCCG-3' and 5'-GCAATAATGGTGGGAACTGCACATGTGGAG-3' was used as a probe for Southern blot analysis. The expression of *RNF8* mRNA was detected by RT-PCR using

the primers 5'-GGCGGCATGGCAGCGTGCGGTGCCTCGAG-3' and 5'-TTACACTGTTTAGATAACGCAGTAGCTTCC-3. Each *RAD18* C29F and *RNF8* C398F knock-in vector was generated from genomic PCR using the following primers.
For *RAD18* C29F,
5'-AGTCAGAAATAAGCGTGGGTGGATATCCGT-3'
5'-GCTGAAGTAATCGAAG***A***AAATCCCACAGC-3' for left arm,
5'-GCTGTGGGATTT***T***CTTCGATTACTTCAGC-3'
5'-CTGGCAGAACTGAAGCTCTTCACTAGCTC-3' for right arm.
Amplified PCR products were cloned into pCR®-Blunt II-TOPO® vector (Invitrogen, CA). The *Eco*RI fragment from this vector was further subcloned into the *Not*I site of the pBluescriptII KS (+) vector. *Not*I site of this vector was used to clone a marker gene (*puro*) cassette.
For *RNF8* C398F,
5'-GGAGTAAAATGGAAAGATGGGGAAGAGAAT-3'
5'-GCTCAGAACAGATTGTG***A***ACTGCAGCTC-3' for left arm,
5'-GAGCTGCAGT***T***CACAATCTGTTCTGAGC-3'
5'-TTAGATAACGCAGTAGCTTCCATTAT-3' for right arm.
Amplified PCR products were cloned into pCR®-Blunt II-TOPO® vector (Invitrogen, CA). *Sca*I site was used to clone a marker gene (*puro*) cassette.
To detect full-length *RNF8* and *RAD18* mRNAs, following primers were used.
For *RNF8*,
5'-ATGGCAGCGTGCGGTGCCTCGAGGCC-3'
5'-TTAGATAACGCAGTAGCTTCCATTAT-3'.
For *RAD18*,
5'-ATGGCCCTGGCGCTGCCCGAACCGC-3'
5'-TCAGCTCTTCTTCCTCTTGCTCCTG-3'.
For the detection of *PCNA* mRNA,
5'-GGGATGTTTGAGGCGCGGCTTGT-3'
5'-CCTCAGTCCCAGTGCAGTTAAGA-3'.

Generation of *RNF8*$^{-/-}$, *RNF8*$^{-/-}$/*KU70*$^{-/-}$, *RAD18*$^{-/-}$/*RNF8*$^{-/-}$, *RAD18* C29F and *RNF8* C398F knock-in mutants

Wild-type DT40 cells were sequentially transfected with the *RNF8-bsr* and the *RNF8-*

puro targeting constructs to obtain *RNF8*$^{-/-}$ cells. The gene-targeting frequency of the stably transfected clones was 50% for the *RNF8*$^{-/+}$ cells and 20% for the *RNF8*$^{-/-}$ clones. The *RNF8-puro* and the *RNF8-neo* targeting constructs were sequentially transfected into *KU70*$^{-/-}$ cells to obtain *RNF8*$^{-/-}$*/KU70*$^{-/-}$ cells. *RAD18*$^{-/-}$ cells were sequentially transfected with the *RNF8-bsr* and the *RNF8-puro* targeting constructs to obtain *RAD18*$^{-/-}$*/RNF8*$^{-/-}$ cells. The establishment of each mutant was confirmed by Southern blotting. To establish *RAD18* C29F and *RNF8* C398F knock-in mutants, each construct described above was transfected into *RAD18*$^{+/-}$ (and *RNF8*$^{-/-}$*/RAD18*$^{+/-}$) or *RNF8*$^{+/-}$ (and *RAD18*$^{-/-}$*/ RNF8*$^{+/-}$), respectively and then gene targeting was validated by PCR. To remove the resistant gene, cells were transfected with the Cre recombinase expression vector and then treated with 0.2μM tamoxifen. 48 hours after the treatment, cells were subcloned and puromycin-sensitive clones were selected.

Chromosome aberration analysis

Karyotype analysis was performed as described previously[34]. For the morphological analysis of chromosome aberrations, cells were treated with colcemid for 3h to enrich for mitotic cells. To count camptothecin-induced chromosomal aberrations, cells were treated with 10nM or 100nM camptothcin for 8h and colcemid was added in the last 3h.

Measurement of cellular sensitivity to DNA-damaging agents

We measured the amount of ATP in cellular lysates to determine the number of live cells [35]. Cells were treated with each DNA-damaging agent in 1ml of medium using 24-well plates and incubated at 39.5°C for 48h (or 72h for olaparib). We transferred 100μl of medium containing the cells to 96-well plates and measured the amount of ATP using CellTiter-Glo (Promega) according to the manufacturer's instructions. Luminescence was measured by Fluoroskan Ascent FL (Thermo Fisher Scientific Inc., Pittsburgh, PA) or ARVO X5 (Perkin Elmer, Inc. Massachusetts, USA).

Immunofluorescent visualization of subnuclear focus formation

The experimental conditions for the immunocytochemical analysis were previously described [28]. Briefly, 30min for FK2 or 1h for Rad51 after irradiation with ^{137}Cs γ-ray (4Gy) or after exposure to camptothecin (40nM) for 1h, DT40 cells (7×10^5 cells/ml)

were collected on a glass slide using Cytospin3 (Shandon, Pittsburgh, PA). Cells were fixed with 4% formaldehyde for 10min at room temperature. After blocking with 3% BSA/PBST, the fixed cells were treated with specific antibodies. Visualization of the Rad51 and FK2 foci was performed as previously described, using the anti-Rad51 rabbit polyclonal antibody (Bioacademia Inc., Osaka, Japan) or the mouse FK2 antibody (Nippon Biotest Laboratories). At least 100 morphologically intact cells were examined.

Human HCT116 cells were grown on coverslips and then washed twice with PBS before fixation. The cells were fixed with 3% paraformaldehyde and permeabilized with 0.5% TritonX-100/PBS. After blocking with 3% goat serum/PBS, the cells were stained with a Rad51 rabbit polyclonal and a 53BP1 mouse monoclonal antibody (BD Bioscience) at 4°C overnight. For secondary staining, we used a goat Alexa555 anti-rabbit (Invitrogen) and a goat Alexa488 anti-mouse antibody (Invitrogen, CA). The DNA was stained with DAPI. The coverslips were mounted with Prolong Gold mounting agent (Invitrogen).

siRNA transfection

The following siRNAs were used in this study: control (MISSION SIC-002, Sigma Genosys), RNF8 (siGENOME, Dharmacon), and BRCA1 5'-GGA ACC UGU CUC CAC AAA GTT-3' (Sigma genosys). RNAi transfection for RNF8 and BRCA1 was performed using Lipofectamin™ RNAiMAX (Invitrogen) in reverse transfection mode.

Western blot analysis of mono-ubiquitylation of PCNA

For the detection of PCNA mono-ubiquitylation, 1×10^7 cells were irradiated with 30 J/m^2 UV and lysed 1.5h post-treatment with Laemli sample buffer and 5% 2-ME and then boiled for 5min followed by ice incubation. 10μl of the sample were run in an SDS-PAGE gel and then proteins were electroblotted onto a PVDF membrane. The following antibodies were used: mouse monoclonal PCNA PC10 (Santa Cruz) and anti-mouse IgG HRP liked (Santa Cruz). Proteins were visualized by Chemi-Lumi One Super (NACALAI TESQUE, INC.).

Conflict of interest

The authors declare no conflict of interest.

Acknowledgements

This work was supported in part by the grants-in-aid program of the Ministry of Education, Sports, and Culture of Japan (for S.T.). We thank Dr. Tadahiro Shiomi and Dr. Naoko Shiomi (National Institute of Radiological Sciences, Japan) for providing us with the HCT116 *RAD18*$^{-/-}$ and *RAD18*$^{+/+}$ cells and Prof. Hitoshi Kurumizaka (Waseda University, Japan) for providing us with the anti-Rad51 antibody. Financial support was provided in part by the Uehara Memorial Foundation, the Naito Foundation, Sumitomo Foundation and Kurata Fundation (for K.H.)**.**

References

1 Yamashita YM, Okada T, Matsusaka T, Sonoda E, Zhao GY, Araki K *et al*. RAD18 and RAD54 cooperatively contribute to maintenance of genomic stability in vertebrate cells. The EMBO journal 2002; 21: 5558-5566.

2 Yoshimura A, Nishino K, Takezawa J, Tada S, Kobayashi T, Sonoda E *et al*. A novel Rad18 function involved in protection of the vertebrate genome after exposure to camptothecin. DNA Repair (Amst) 2006; 5: 1307-1316.

3 Saberi A, Hochegger H, Szuts D, Lan L, Yasui A, Sale JE *et al*. RAD18 and poly(ADP-ribose) polymerase independently suppress the access of nonhomologous end joining to double-strand breaks and facilitate homologous recombination-mediated repair. Mol Cell Biol 2007; 27: 2562-2571.

4 Takata M, Sasaki MS, Sonoda E, Morrison C, Hashimoto M, Utsumi H *et al*. Homologous recombination and non-homologous end-joining pathways of DNA double-strand break repair have overlapping roles in the maintenance of chromosomal integrity in vertebrate cells. The EMBO journal 1998; 17: 5497-5508.

5 Pommier Y. Topoisomerase I inhibitors: camptothecins and beyond. Nature reviews 2006; 6: 789-802.

6 Bryant HE, Schultz N, Thomas HD, Parker KM, Flower D, Lopez E *et al*. Specific killing of BRCA2-deficient tumours with inhibitors of poly(ADP-ribose) polymerase. Nature 2005; 434: 913-917.

7 Adachi N, So S, Koyama H. Loss of nonhomologous end joining confers camptothecin resistance in DT40 cells. Implications for the repair of topoisomerase I-mediated DNA damage. J Biol Chem 2004; 279: 37343-37348.

8 Farmer H, McCabe N, Lord CJ, Tutt AN, Johnson DA, Richardson TB *et al*. Targeting the DNA repair defect in BRCA mutant cells as a therapeutic strategy.

Nature 2005; 434: 917-921.

9 Hochegger H, Dejsuphong D, Fukushima T, Morrison C, Sonoda E, Schreiber V *et al*. Parp-1 protects homologous recombination from interference by Ku and Ligase IV in vertebrate cells. The EMBO journal 2006; 25: 1305-1314.

10 Bunting SF, Callen E, Wong N, Chen HT, Polato F, Gunn A *et al*. 53BP1 inhibits homologous recombination in Brca1-deficient cells by blocking resection of DNA breaks. Cell 2010; 141: 243-254.

11 Li L, Halaby MJ, Hakem A, Cardoso R, El Ghamrasni S, Harding S *et al*. Rnf8 deficiency impairs class switch recombination, spermatogenesis, and genomic integrity and predisposes for cancer. J Exp Med 2010; 207: 983-997.

12 Santos MA, Huen MS, Jankovic M, Chen HT, Lopez-Contreras AJ, Klein IA *et al*. Class switching and meiotic defects in mice lacking the E3 ubiquitin ligase RNF8. J Exp Med 2010; 207: 973-981.

13 Lu LY, Wu J, Ye L, Gavrilina GB, Saunders TL, Yu X. RNF8-dependent histone modifications regulate nucleosome removal during spermatogenesis. Dev Cell 2010; 18: 371-384.

14 Sun J, Yomogida K, Sakao S, Yamamoto H, Yoshida K, Watanabe K *et al*. Rad18 is required for long-term maintenance of spermatogenesis in mouse testes. Mech Dev 2009; 126: 173-183.

15 Wu J, Chen Y, Lu LY, Wu Y, Paulsen MT, Ljungman M *et al*. Chfr and RNF8 synergistically regulate ATM activation. Nat Struct Mol Biol 2011; 18: 761-768.

16 Zhao GY, Sonoda E, Barber LJ, Oka H, Murakawa Y, Yamada K *et al*. A critical role for the ubiquitin-conjugating enzyme Ubc13 in initiating homologous recombination. Mol Cell 2007; 25: 663-675.

17 Yamazoe M, Sonoda E, Hochegger H, Takeda S. Reverse genetic studies of the DNA damage response in the chicken B lymphocyte line DT40. DNA Repair (Amst) 2004; 3: 1175-1185.

18 Yamamoto M, Okamoto T, Takeda K, Sato S, Sanjo H, Uematsu S *et al*. Key function for the Ubc13 E2 ubiquitin-conjugating enzyme in immune receptor signaling. Nat Immunol 2006; 7: 962-970.

19 Fukushima T, Matsuzawa S, Kress CL, Bruey JM, Krajewska M, Lefebvre S *et al*. Ubiquitin-conjugating enzyme Ubc13 is a critical component of TNF receptor-associated factor (TRAF)-mediated inflammatory responses. Proc Natl Acad Sci U S A 2007; 104: 6371-6376.

20 Adachi N, Suzuki H, Iiizumi S, Koyama H. Hypersensitivity of nonhomologous DNA end-joining mutants to VP-16 and ICRF-193: implications for the repair of topoisomerase II-mediated DNA damage. J Biol Chem 2003; 278: 35897-35902.

21 Maede Y, Shimizu H, Fukushima T, Kogame T, Nakamura T, Miki T *et al*. Differential and Common DNA Repair Pathways for Topoisomerase I- and II-Targeted Drugs in a Genetic DT40 Repair Cell Screen Panel. Mol Cancer Ther 2014; 13: 214-220.

22 Oestergaard VH, Pentzold C, Pedersen RT, Iosif S, Alpi A, Bekker-Jensen S *et al*. RNF8 and RNF168 but not HERC2 are required for DNA damage-induced ubiquitylation in chicken DT40 cells. DNA Repair (Amst) 2012; 11: 892-905.

23 Mailand N, Bekker-Jensen S, Faustrup H, Melander F, Bartek J, Lukas C *et al*. RNF8 ubiquitylates histones at DNA double-strand breaks and promotes assembly of repair proteins. Cell 2007; 131: 887-900.

24 Kolas NK, Chapman JR, Nakada S, Ylanko J, Chahwan R, Sweeney FD *et al*. Orchestration of the DNA-damage response by the RNF8 ubiquitin ligase. Science 2007; 318: 1637-1640.

25 Huen MS, Grant R, Manke I, Minn K, Yu X, Yaffe MB *et al*. RNF8 transduces the DNA-damage signal via histone ubiquitylation and checkpoint protein assembly. Cell 2007; 131: 901-914.

26 Huang J, Huen MS, Kim H, Leung CC, Glover JN, Yu X *et al*. RAD18 transmits DNA damage signalling to elicit homologous recombination repair. Nat Cell Biol 2009; 11: 592-603.

27 Luijsterburg MS, Acs K, Ackermann L, Wiegant WW, Bekker-Jensen S, Larsen DH *et al*. A new non-catalytic role for ubiquitin ligase RNF8 in unfolding higher-order chromatin structure. The EMBO journal 2012; 31: 2511-2527.

28 Takata M, Sasaki MS, Tachiiri S, Fukushima T, Sonoda E, Schild D *et al*. Chromosome instability and defective recombinational repair in knockout mutants of the five Rad51 paralogs. Mol Cell Biol 2001; 21: 2858-2866.

29 Lu CS, Truong LN, Aslanian A, Shi LZ, Li Y, Hwang PY *et al*. The RING finger protein RNF8 ubiquitinates Nbs1 to promote DNA double-strand break repair by homologous recombination. J Biol Chem 2012; 287: 43984-43994.

30 Inagaki A, van Cappellen WA, van der Laan R, Houtsmuller AB, Hoeijmakers JH, Grootegoed JA *et al*. Dynamic localization of human RAD18 during the cell cycle and a functional connection with DNA double-strand break repair. DNA Repair (Amst) 2009; 8: 190-201.

31 Chapman JR, Taylor MR, Boulton SJ. Playing the end game: DNA double-strand break repair pathway choice. Mol Cell 2012; 47: 497-510.

32 Watanabe K, Iwabuchi K, Sun J, Tsuji Y, Tani T, Tokunaga K *et al*. RAD18 promotes DNA double-strand break repair during G1 phase through chromatin retention of 53BP1. Nucleic Acids Res 2009; 37: 2176-2193.

33 Palle K, Vaziri C. Rad18 E3 ubiquitin ligase activity mediates Fanconi anemia pathway activation and cell survival following DNA Topoisomerase 1 inhibition. Cell Cycle 2011; 10: 1625-1638.

34 Sonoda E, Sasaki MS, Buerstedde JM, Bezzubova O, Shinohara A, Ogawa H *et al*. Rad51-deficient vertebrate cells accumulate chromosomal breaks prior to cell death. The EMBO journal 1998; 17: 598-608.

35 Ji K, Kogame T, Choi K, Wang X, Lee J, Taniguchi Y *et al*. A novel approach using DNA-repair-deficient chicken DT40 cell lines for screening and characterizing the genotoxicity of environmental contaminants. Environ Health Perspect 2009; 117: 1737-1744.

Table 1 **DT40 mutants used in this study**

Cell line	Selection marker for gene disruption First gene	Second gene	Reference
RNF8$^{-/-}$	*bsr/puro*		This study
UBC13$^{-/-}$	*bsr/his*		16
RAD18$^{-/-}$	*his/hygro*		1, 3
RAD18$^{-/-}$*/RNF8*$^{-/-}$	*his/hygro*	*bsr/puro*	This study
KU70$^{-/-}$	*his/bsr*		4
RNF8$^{-/-}$*/KU70*$^{-/-}$	*his/bsr*	*puro/neo*	This study
RAD18$^{-/-}$*/KU70*$^{-/-}$	*puro/hygro*	*his/bsr*	3
RNF8$^{C398F/-}$	*bsr*/ Cre-excised *puro*		This study
RAD18$^{C29F/-}$	*neo*/ Cre-excised *puro*		This study
RAD18$^{-/-}$*/RNF8*$^{C398F/-}$	*his/hygro*	*bsr*/ Cre-excised *puro*	This study
RNF8$^{-/-}$*/RAD18*$^{C29F/-}$	Cre-excised both *bsr* and *puro*	*neo*/ Cre-excised *puro*	This study

Figure Legends

Figure 1. ***RNF8*$^{-/-}$ and *UBC13*$^{-/-}$ cells display distinctly different phenotypes**
(A) The average doubling time for the indicated genotypes. Error bars show the standard error in at least three independent experiments. (B) Spontaneously arising chromosomal aberrations in 50 mitotic cells. Two breaks at the same site of both sister chromatids are defined as chromosome-type breaks (white rectangle), while breaks at one of two sister chromatids are chromatid-type (gray rectangle). (C-E) Cellular sensitivity to ICRF193 (C), camptothecin (D), and olaparib (E) was analyzed. Survival rate was calculated as the percentage of surviving cells treated with DNA-damaging agents relative to the untreated surviving cells. The concentration or dose is displayed on the horizontal axis on a linear scale, while the survival rate is displayed on the y-axis on a logarithmic scale. Error bars show the standard error of the mean in at least three independent experiments.

Figure 2. **The Rad18 and Rnf8 ubiquitin ligases operate in the same pathway in cellular tolerance to camptothecin and olaparib, while they promote Rad51 recruitment to γ-ray-induced DSB sites independently of each other**
(A-D) Cellular survival of the indicated DNA damaging agents is shown as in Figure 1. ICRF193 (A), camptothecin (B), olaparib (C), and ionizing radiation (^{137}Cs γ-ray) (D). (E) The average number of γ-ray-induced Rad51 foci per cell. Cells were fixed 1h after 4Gy γ-rays irradiation and then stained with anti-Rad51 antibody. Each histogram represents the value obtained by subtracting the number of Rad51 foci in non-irradiated controls from observed foci 1h after irradiation. The actual number of the number of Rad51 foci is shown in Supplementary Figure 2B. 100 to 200 cells were counted and error bars represent standard error calculated from at least three independent experiments. Statistical significance was determined by a Student's *t*-test: P (*) < 0.01. (F) HCT116 cells transfected with the indicated siRNAs were exposed to 2Gy ionizing radiation. Six hours after irradiation (IR), cells were fixed and subjected to Rad51 and 53BP1 immunofluorescence analysis. Cells treated with siRNA for 2 days were used in this experiment. Depletion of RNF8 was assessed by the disappearance of 53BP1 foci (Supplementary Figure 3). Cells with >3 Rad51 foci were counted as positive cells. 300 cells were counted. Data are represented as the mean ± SD (n = 3).

Figure 3. **Collaboration between Rad18 and Rnf8 suppresses the toxic effect of NHEJ on HR and contributes to the cellular tolerance to camptothecin and olaparib**

(A, B) Cellular sensitivity to camptothecin (A), olaparib (B) and γ-rays (D) is shown as in Figure 1. Lethal dose 30% (LD30) is the concentration of DNA damaging agents that reduces cellular survival to 30% relative to cells non-treated with DNA damaging agents. (C) Chromosomal aberrations in cells treated with 10nM camptothecin. The data represent the mean and SD from three independent counts each analyzing 50 mitotic cells. (D) The average number of Rad51 foci per cell in camptothecin-treated cells. Cells were exposed to 40nM camptothecin for 1hr, and then stained with anti-Rad51 antibody. Each histogram represents the value obtained by subtracting the number of Rad51 foci in non-irradiated controls from observed foci 1h after irradiation. The actual number of Rad51 foci is shown in Supplementary Figure 2A and B. 100 to 200 cells were counted in each experiment, and error bars represent standard error calculated from at least three independent experiments. *P*-value was calculated by a student's *t*-test: *P* (*) <0.01 and NS (not significant). (E) Representative images of radial chromosomes are shown. Arrows indicate radial chromosomes. (F) Formation of radial chromosomes in cells treated with 100nM camptothecin. The data represent the mean and SD from three independent experiments each analyzing 200 mitotic cells. *P*-value was calculated by a student's *t*-test: *P* (*) <0.01, (**) *P*<0.05, and NS (not significant).

Figure 4. **The ubiquitylation activity of Rad18 and Rnf8 is essential for cellular tolerance to camptothecin, olaparib and ionizing radiation**

(A–C) Cellular sensitivity to camptothecin (A), olaparib (B), and ionizing radiation (C) is shown as in Figure 1. Error bars represent the standard error of the mean in at least three independent experiments. (D) The average number of Rad51 foci at 1h after γ-rays irradiation. More than 100 cells were counted in each experiment and the data represent the mean and standard error from at least three independent experiments. *P* (*) <0.01, (**) <0.05, and NS (not significant).

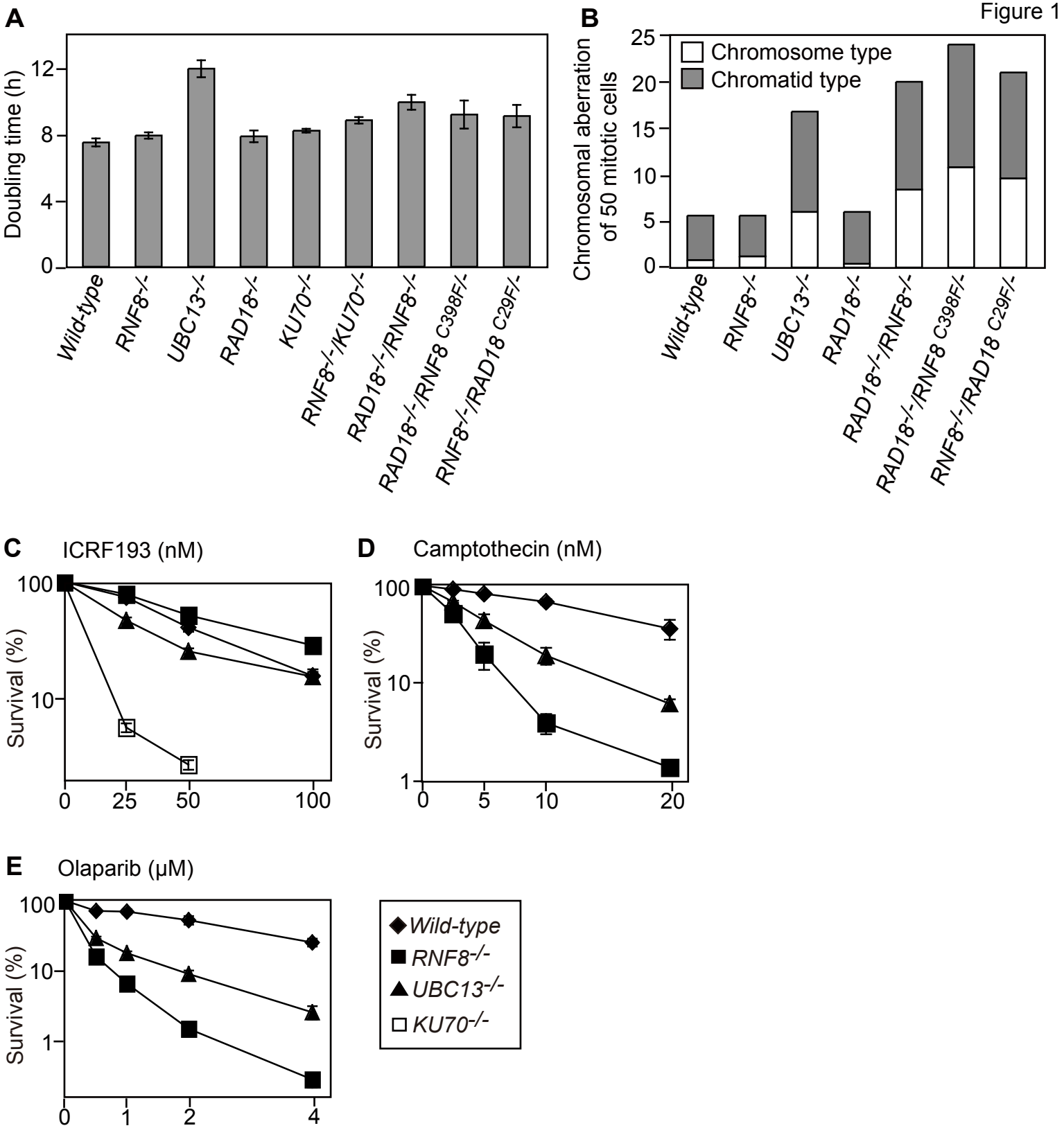
A
Doubling time (h)
0
4
8
12
Wild-type
RNF8-/-
UBC13-/-
RAD18-/-
KU70-/-
RNF8-/-/KU70-/-
RAD18-/-/RNF8-/-
RAD18-/-/RNF8 C398F/-
RNF8-/-/RAD18 C29F/-
B
Chromosomal aberration of 50 mitotic cells
Chromosome type
Chromatid type
0
5
10
15
20
25
Wild-type
RNF8-/-
UBC13-/-
RAD18-/-
RAD18-/-/RNF8-/-
RAD18-/-/RNF8 C398F/-
RNF8-/-/RAD18 C29F/-
C
ICRF193 (nM)
Survival (%)
100
10
0
25
50
100
D
Camptothecin (nM)
Survival (%)
100
10
1
0
5
10
20
E
Olaparib (μM)
Survival (%)
100
10
1
0
1
2
4
Wild-type
RNF8-/-
UBC13-/-
KU70-/-

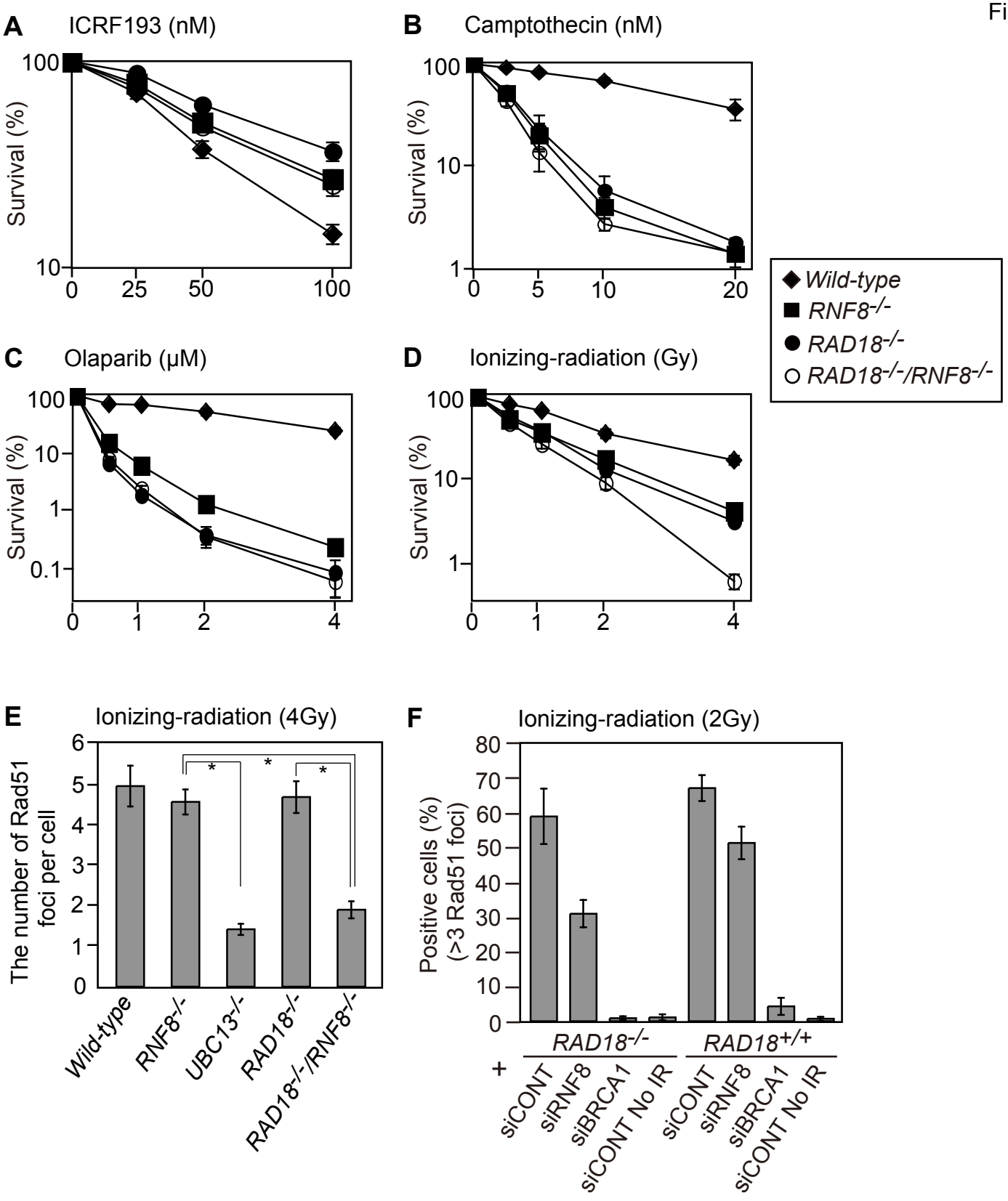
A
ICRF193 (nM)
Survival (%)
100
10
0
25
50
100
B
Camptothecin (nM)
Survival (%)
100
10
1
0
5
10
20
Wild-type
RNF8-/-
RAD18-/-
RAD18-/-/RNF8-/-
C
Olaparib (μM)
Survival (%)
100
10
1
0.1
0
1
2
4
D
Ionizing-radiation (Gy)
Survival (%)
100
10
1
0
1
2
4
E
Ionizing-radiation (4Gy)
The number of Rad51 foci per cell
6
5
4
3
2
1
0
*
*
*
Wild-type
RNF8-/-
UBC13-/-
RAD18-/-
RAD18-/-/RNF8-/-
F
Ionizing-radiation (2Gy)
Positive cells (%) (>3 Rad51 foci)
80
70
60
50
40
30
20
10
0
RAD18-/-
RAD18+/+
+
siCONT
siRNF8
siBRCA1
siCONT No IR
siCONT
siRNF8
siBRCA1
siCONT No IR

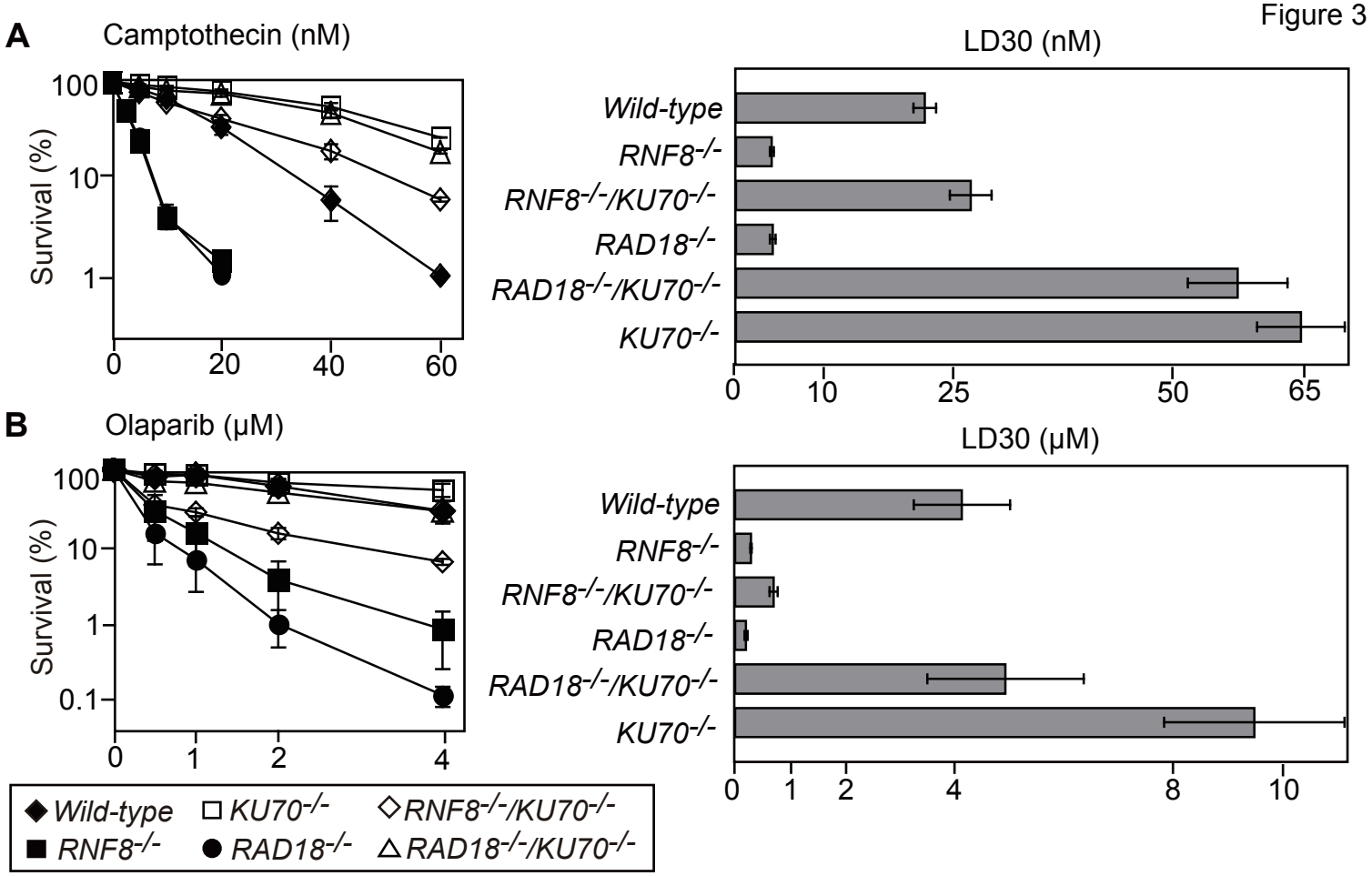
A
Camptothecin (nM)
Survival (%)
100
10
1
0
20
40
60
LD30 (nM)
Wild-type
RNF8-/-
RNF8-/-/KU70-/-
RAD18-/-
RAD18-/-/KU70-/-
KU70-/-
0
10
25
50
65
B
Olaparib (μM)
Survival (%)
100
10
1
0.1
0
1
2
4
LD30 (μM)
Wild-type
RNF8-/-
RNF8-/-/KU70-/-
RAD18-/-
RAD18-/-/KU70-/-
KU70-/-
0
1
2
4
8
10
Wild-type
KU70-/-
RNF8-/-/KU70-/-
RNF8-/-
RAD18-/-
RAD18-/-/KU70-/-

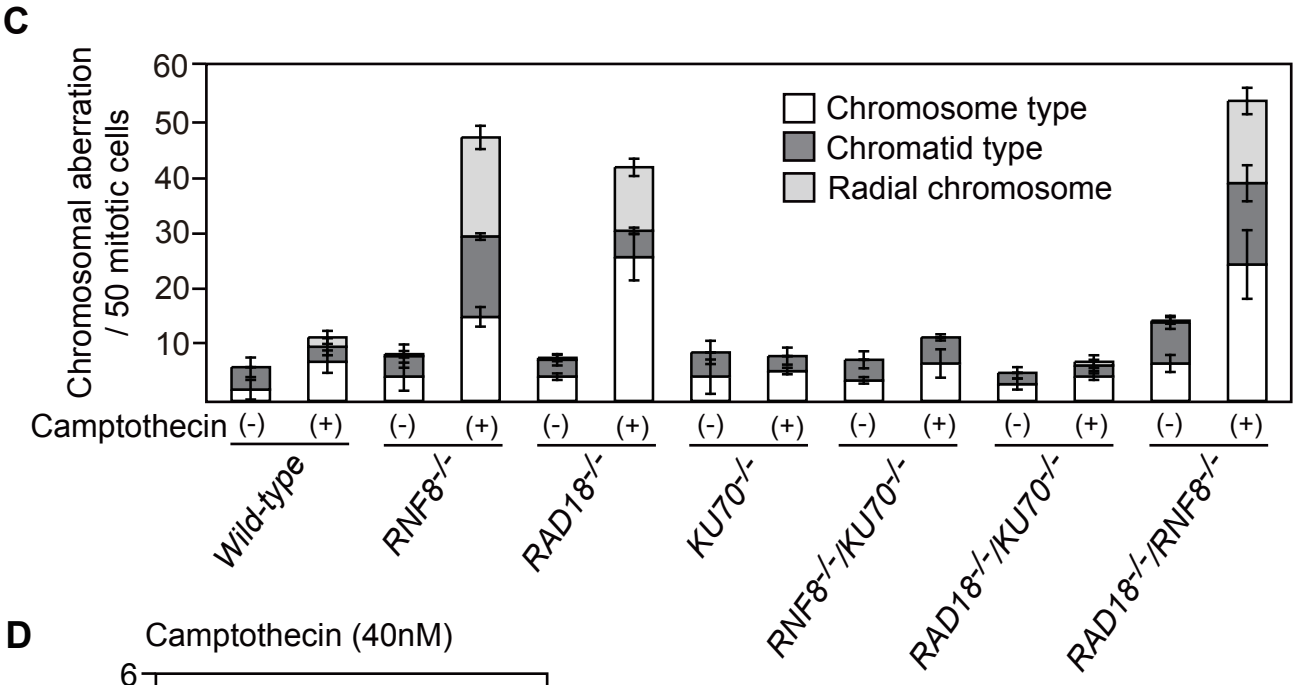
C
Chromosomal aberration / 50 mitotic cells
60
50
40
30
20
10
Chromosome type
Chromatid type
Radial chromosome
Camptothecin
(-)
(+)
Wild-type
RNF8-/-
RAD18-/-
KU70-/-
RNF8-/-/KU70-/-
RAD18-/-/KU70-/-
RAD18-/-/RNF8-/-

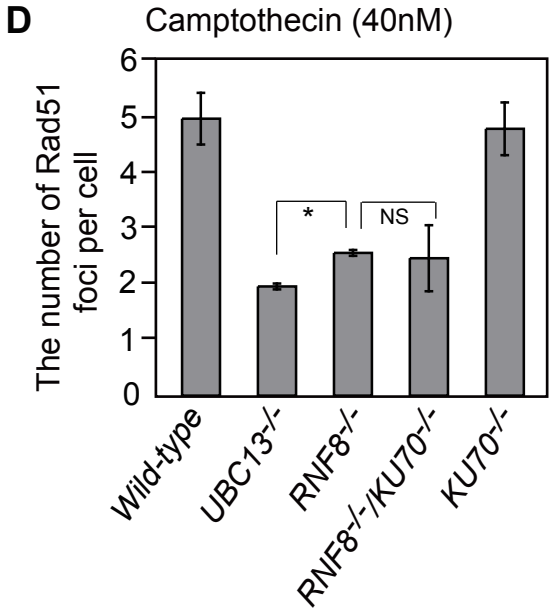
D
Camptothecin (40nM)
The number of Rad51 foci per cell
6
5
4
3
2
1
0
*
NS
Wild-type
UBC13-/-
RNF8-/-
RNF8-/-/KU70-/-
KU70-/-

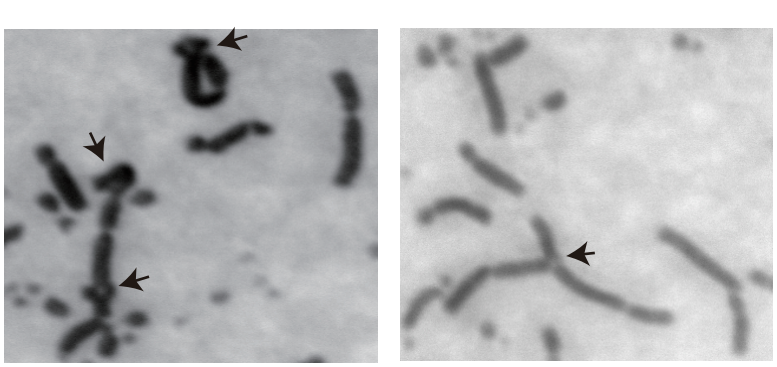
E

F

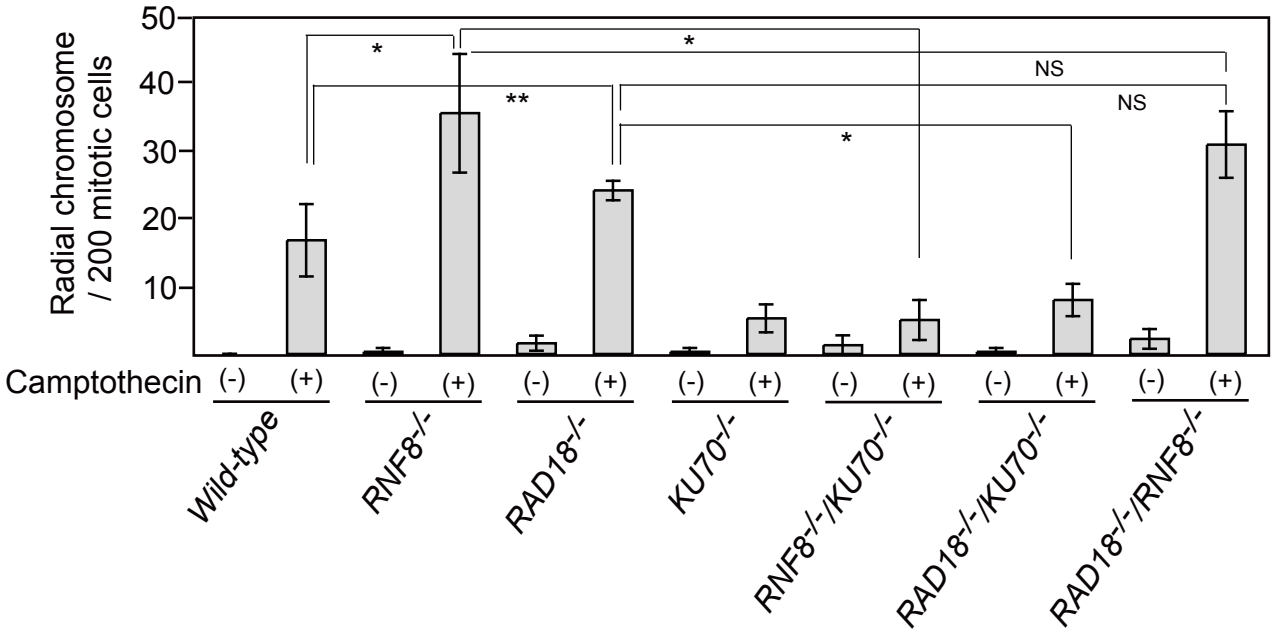
Radial chromosome / 200 mitotic cells
50
40
30
20
10
*
**
*
*
NS
NS
Camptothecin (-) (+) (-) (+) (-) (+) (-) (+) (-) (+) (-) (+) (-) (+)
Wild-type
RNF8-/-
RAD18-/-
KU70-/-
RNF8-/-/KU70-/-
RAD18-/-/KU70-/-
RAD18-/-/RNF8-/-

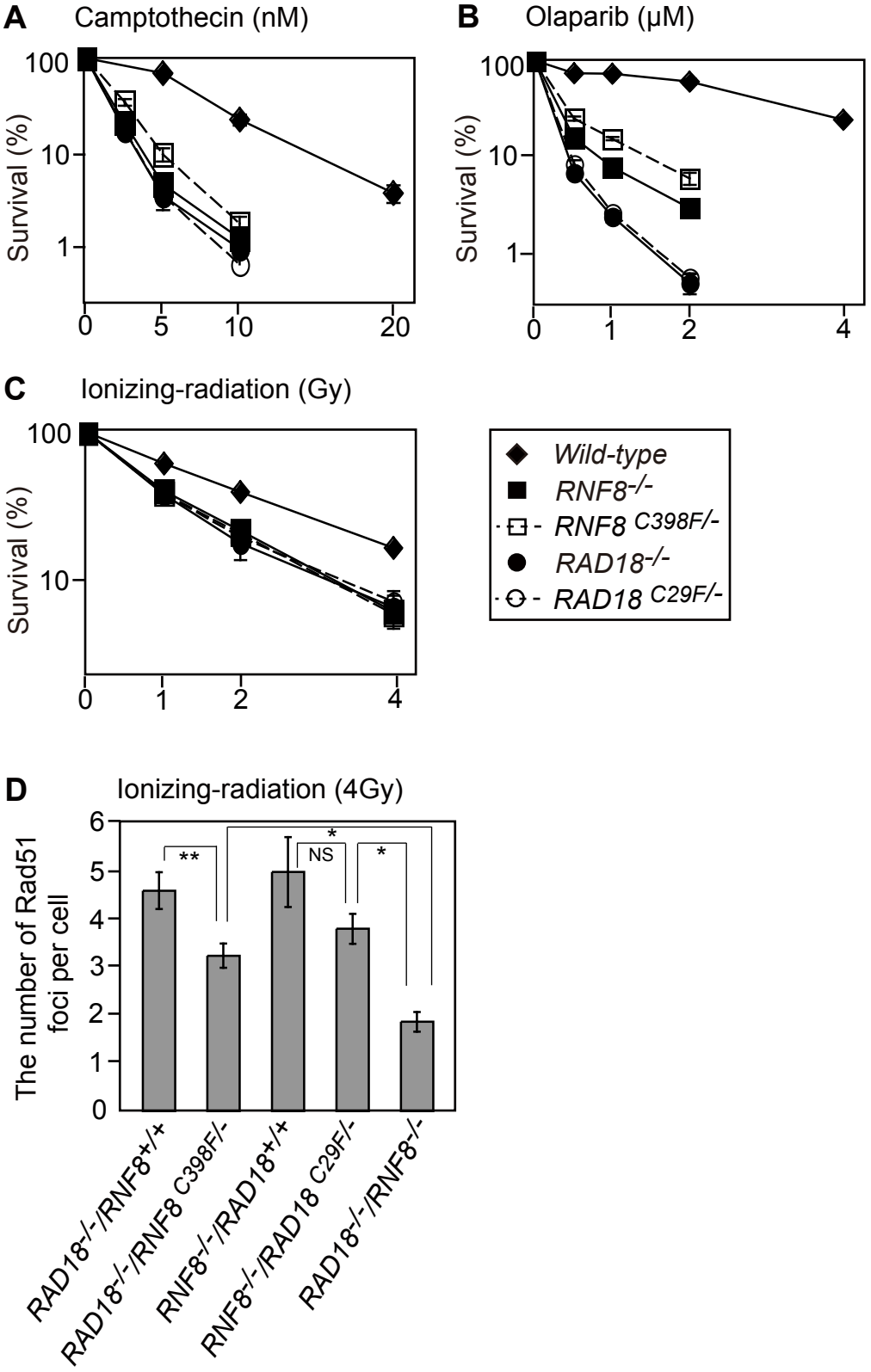
A
Camptothecin (nM)
Survival (%)
100
10
1
0
5
10
20
B
Olaparib (μM)
Survival (%)
100
10
1
0
1
2
4
C
Ionizing-radiation (Gy)
Survival (%)
100
10
0
1
2
4
Wild-type
RNF8-/-
RNF8 C398F/-
RAD18-/-
RAD18 C29F/-
D
Ionizing-radiation (4Gy)
The number of Rad51 foci per cell
6
5
4
3
2
1
0
**
NS
*
*
RAD18-/-/RNF8+/+
RAD18-/-/RNF8 C398F/-
RNF8-/-/RAD18+/+
RNF8-/-/RAD18 C29F/-
RAD18-/-/RNF8-/-

Supplementary Figure 1. **Gene-targeting at the *RNF8* locus**

(A) Schematic representation of part of the *RNF8* locus, the gene-disruption constructs, and the configuration of the targeted alleles. Solid boxes indicate the position of exons. Relevant *Xba*I recognition sites for the genomic Southern blot analysis are indicated with *X*. The indicated probe was used for the Southern blot analysis in (B). (B) Southern blot analysis of *Xba*I-digested genomic DNA from cells with the indicated genotypes of the *RNF8* gene. The positions and sizes of hybridizing fragments of *wild-type* (14 kb) and targeted loci (6.5 kb and 5.4 kb) are indicated. (C) RT-PCR results for the indicated genotypes of the *RNF8* gene. *PCNA* was used as a positive control. (D-F) Cellular sensitivity to camptothecin (D), olaparib (E), and ionizing radiation (F) was analyzed. Error bars show the standard error of the mean in at least three independent experiments.

Supplementary Figure 2. **The generation of *RNF8*$^{C398F/-}$ cells**

(A) Schematic representation of *RNF8* C398F knock-in construct. After the generation of *RNF8*$^{C398F(puro)/-(bsr)}$ cells, the cells were transfected with a Cre recombinase expression vector and treated with tamoxifen to remove the *puro* resistant gene. (B) RT-PCR results for the indicated genotypes of the *RNF8* gene. *PCNA* was used as a positive control. (C) The representative image of FK2 immunostaining at 30min after 4Gy γ-rays irradiation. Blue and red represent DAPI and FK2, respectively.

Supplementary Figure 3. **The generation of *RAD18*$^{C29F/-}$ cells**

(A) Schematic representation of *RAD18* C29F knock-in construct. After the generation of *RAD18*$^{C29F(puro)/-(neo)}$ cells, the cells were transfected with a Cre recombinase expression vector and treated with tamoxifen to remove the *puro* resistant gene. (B) RT-PCR results for the indicated genotypes of the *RAD18* gene. *PCNA* was used as a positive control. (C) Analysis of mono-ubiquitylation of PCNA. Cells were irradiated with 30J/m^2 UV and then incubated for 1.5h. Protein extracts were prepared in native conditions for mono-ubiquitylation of PCNA and analyzed by SDS-PAGE followed by western blotting using an anti-PCNA antibody. PCNA (short exposure) was used as a loading control.

Supplementary Figure 4. **Quantification of Rad51 focus formation**

(A) The average number of Rad51 foci with or without camptothecin treatment in Figure 3D. (B) The average number of Rad51 foci with or without γ-rays irradiation in Figure 2E and 4D.

Supplementary Figure 5. **Representative images of Rad51 and 53BP1 foci following siRNAs treatment and IR irradiation.** The representative images of Rad51 and 53BP1 foci of Figure 2F.

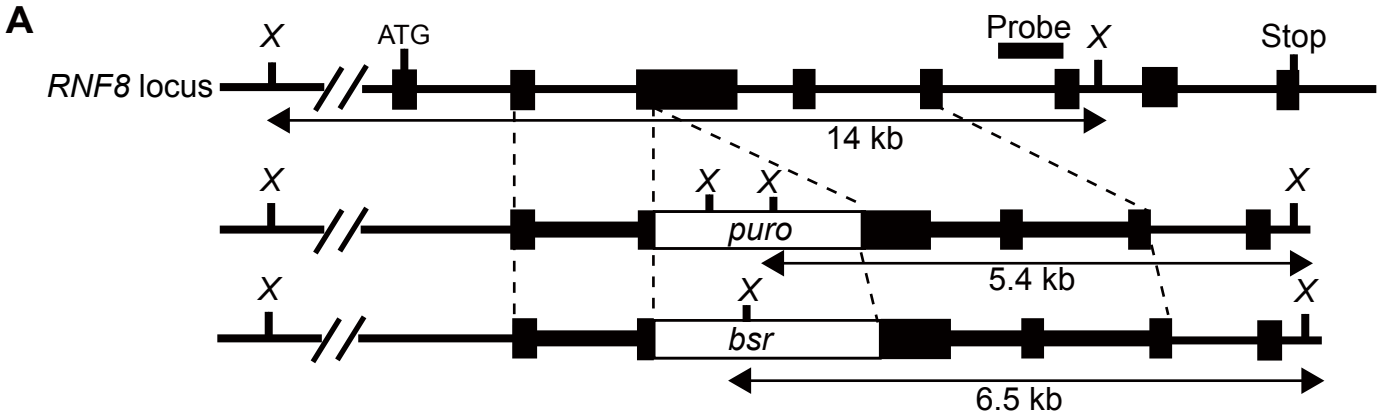
A
RNF8 locus
X
ATG
Probe
X
Stop
14 kb
X
X
X
X
puro
5.4 kb
X
X
X
bsr
6.5 kb

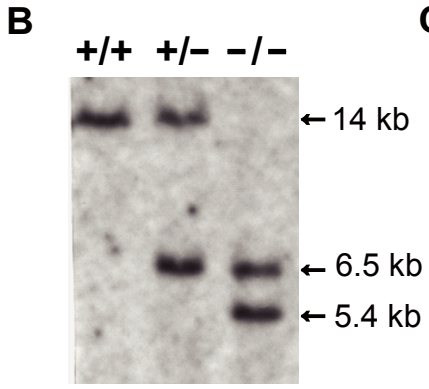
B
+/+
+/−
−/−
14 kb
6.5 kb
5.4 kb

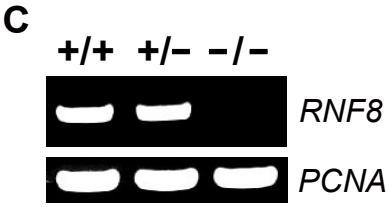
C
+/+
+/−
−/−
RNF8
PCNA

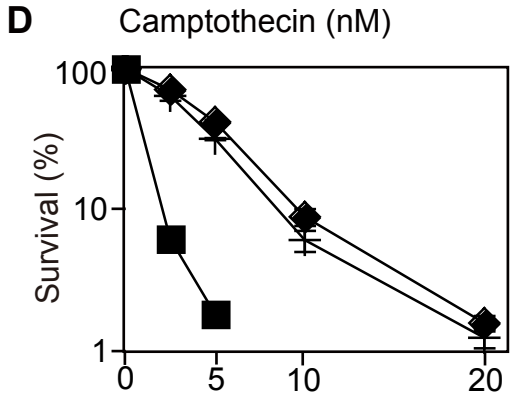
D
Camptothecin (nM)
Survival (%)
100
10
1
0
5
10
20

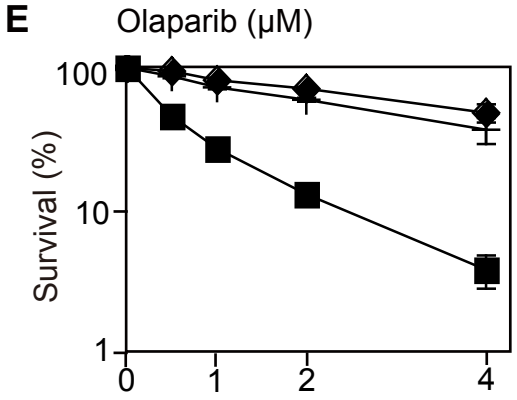
E
Olaparib (μM)
Survival (%)
100
10
1
0
1
2
4

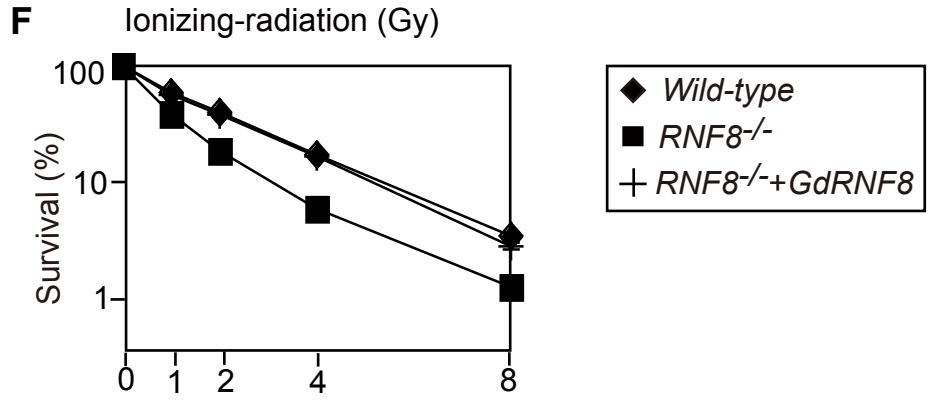
F
Ionizing-radiation (Gy)
Survival (%)
100
10
1
0
1
2
4
8
Wild-type
RNF8-/-
RNF8-/-+GdRNF8

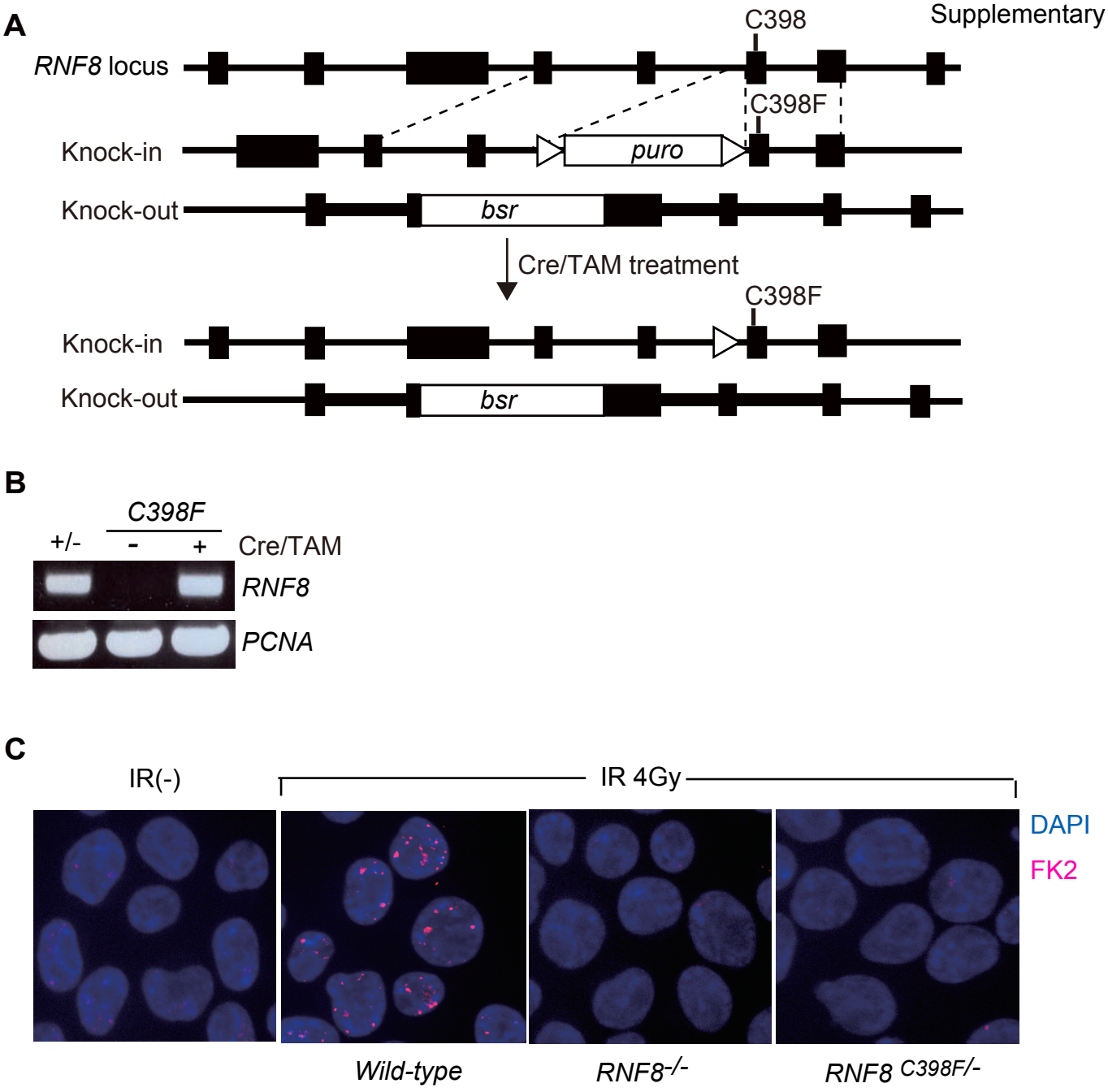
A
C398
RNF8 locus
C398F
Knock-in
puro
Knock-out
bsr
Cre/TAM treatment
C398F
Knock-in
Knock-out
bsr
B
C398F
+/-
-
+
Cre/TAM
RNF8
PCNA
C
IR(-)
IR 4Gy
DAPI
FK2
Wild-type
RNF8-/-
RNF8 C398F/-

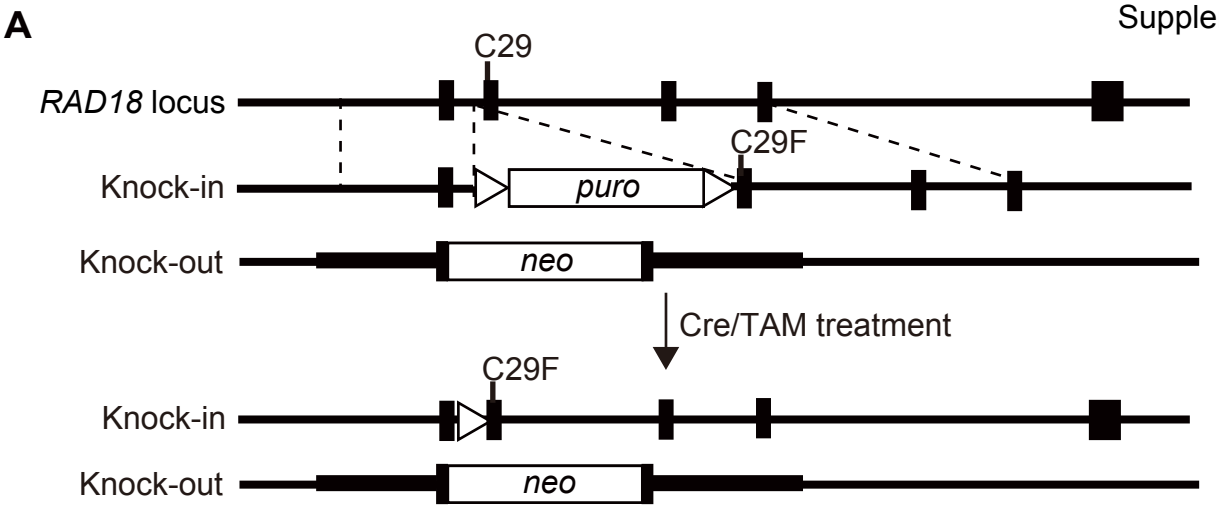
A
C29
RAD18 locus
C29F
Knock-in
puro
Knock-out
neo
Cre/TAM treatment
C29F
Knock-in
Knock-out
neo

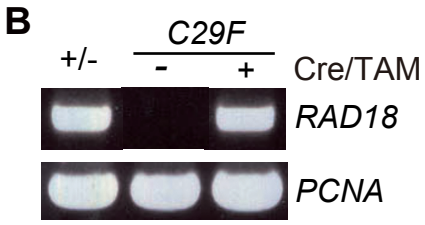
B
C29F
+/-
-
+
Cre/TAM
RAD18
PCNA

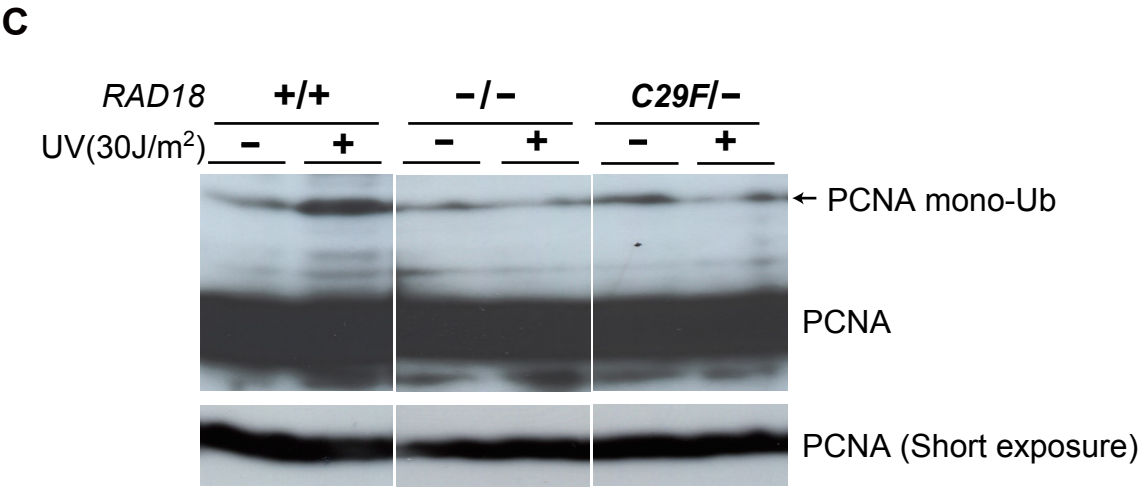
C
RAD18
+/+
−/−
C29F/−
UV(30J/m2)
−
+
−
+
−
+
← PCNA mono-Ub
PCNA
PCNA (Short exposure)

A

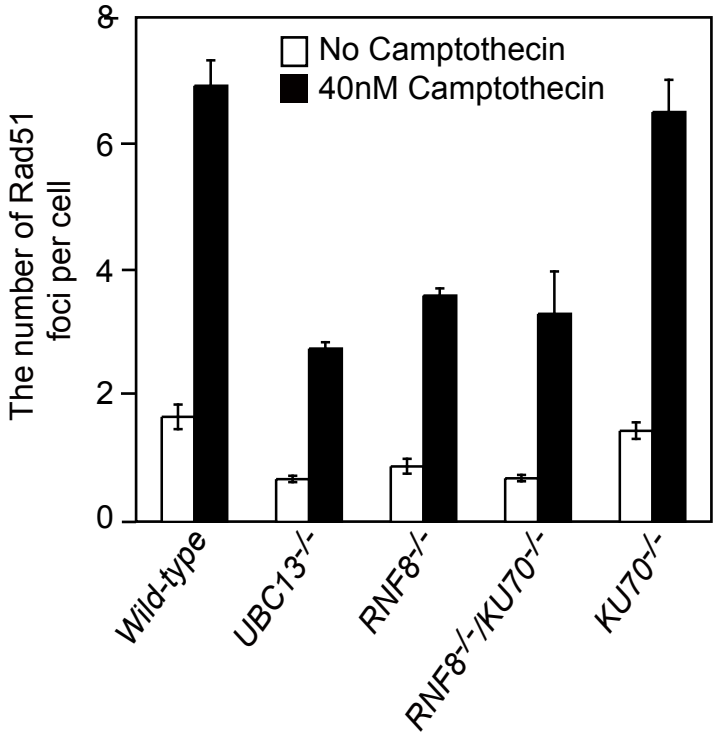
No Camptothecin
40nM Camptothecin
The number of Rad51 foci per cell
0
2
4
6
8
Wild-type
UBC13-/-
RNF8-/-
RNF8-/-/KU70-/-
KU70-/-

B

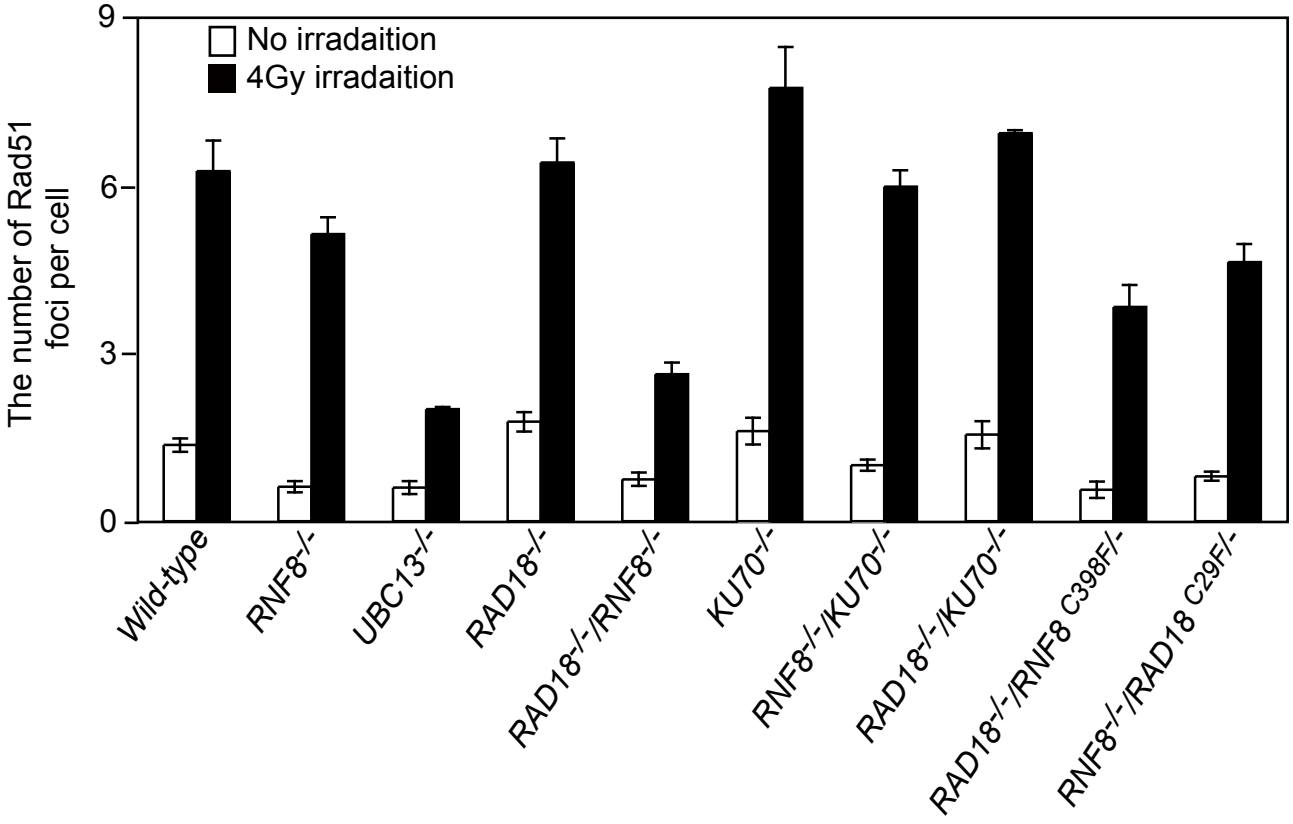
No irradaition
4Gy irradaition
The number of Rad51 foci per cell
0
3
6
9
Wild-type
RNF8-/-
UBC13-/-
RAD18-/-
RAD18-/-/RNF8-/-
KU70-/-
RNF8-/-/KU70-/-
RAD18-/-/KU70-/-
RAD18-/-/RNF8 C398F/-
RNF8-/-/RAD18 C29F/-

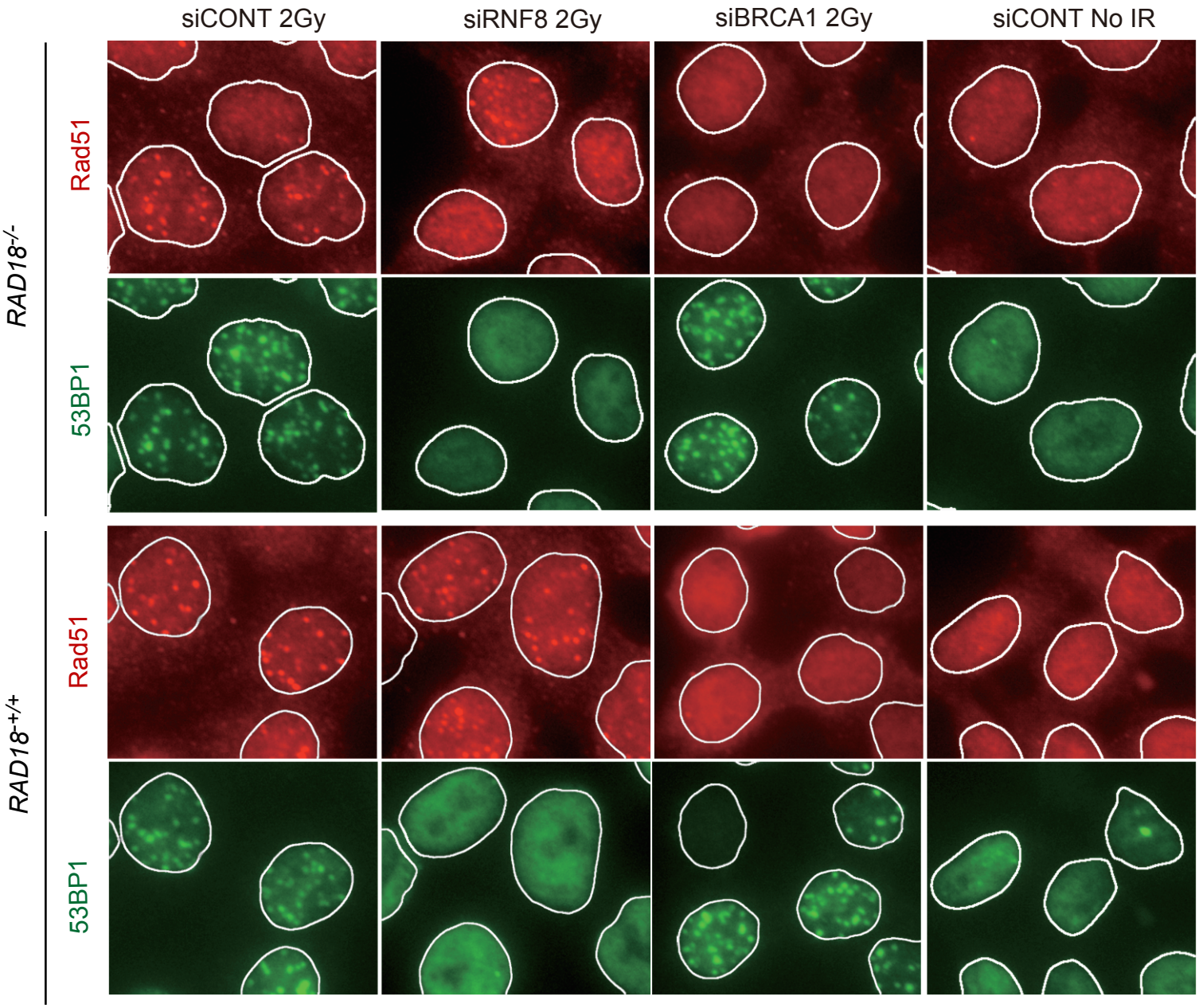
siCONT 2Gy
siRNF8 2Gy
siBRCA1 2Gy
siCONT No IR
RAD18-/-
Rad51
53BP1
RAD18+/+
Rad51
53BP1